Principle of radial transport in low temperature annular plasmas

Yunchao Zhang, Christine Charles, and Rod Boswell

Citation: Physics of Plasmas **22**, 073510 (2015); doi: 10.1063/1.4927461
View online: http://dx.doi.org/10.1063/1.4927461
View Table of Contents: http://scitation.aip.org/content/aip/journal/pop/22/7?ver=pdfcov
Published by the AIP Publishing

Principle of radial transport in low temperature annular plasmas

Yunchao Zhang,[a] Christine Charles, and Rod Boswell
Space Plasma, Power and Propulsion Laboratory, Research School of Physics and Engineering, The Australian National University, Bldg 60, Mills Road, Australian Capital Territory 2601, Australia

(Received 28 April 2015; accepted 3 July 2015; published online 24 July 2015)

Radial transport in low temperature annular plasmas is investigated theoretically in this paper. The electrons are assumed to be in quasi-equilibrium due to their high temperature and light inertial mass. The ions are not in equilibrium and their transport is analyzed in three different situations: a low electric field (LEF) model, an intermediate electric field (IEF) model, and a high electric field (HEF) model. The universal IEF model smoothly connects the LEF and HEF models at their respective electric field strength limits and gives more accurate results of the ion mobility coefficient and effective ion temperature over the entire electric field strength range. Annular modelling is applied to an argon plasma and numerical results of the density peak position, the annular boundary loss coefficient and the electron temperature are given as functions of the annular geometry ratio and Paschen number. © *2015 AIP Publishing LLC*.
[http://dx.doi.org/10.1063/1.4927461]

I. INTRODUCTION

A cylindrical plasma is made annular when an inner object is inserted and this implementation is widely seen in low temperature plasma applications ranging from the probe within a plasma column[1,2] to the inner quartz tube in a plasma source,[3–5] or the central electrode in a plasma jet.[6,7] Two dimensional fluid simulations (no azimuthal flow) for a cylindrical plasma[8,9] have shown that, by using the variable separation technique, the partial differential equation (PDE) for the momentum conservation can be separated into the forms of two ordinary differential equations (ODEs) in the axial and radial directions. The two ODEs are weakly coupled through the drag term caused by the ionization frequency from the particle conservation. When either (axial or radial) dimension is the main interest for a specific plasma system, the other dimension may be assumed to be "frozen," i.e., a quiescent or constant plasma flux such that no plasma loss occurs in this dimension. Then, the primarily concerned dimension can be separately solved at the cost of some loss in accuracy which depends on the specific flow in the assumed frozen dimension. This methodology has been widely applied in a number of modelling studies[10–12] and its validity has also been verified by experiments.[13–15] Axial transport in an annular plasma is similar to that in a cylindrical plasma. The implementation of an inner cylinder in a cylindrical plasma does not change the axial boundary condition and has a small effect on the axial flow except for the value of the coupled drag term. However, radial transport in an annular plasma is quite different from that in a cylindrical plasma. The annular geometry greatly affects the radial boundary conditions: a cylindrical plasma has a central point of maximum ion density and zero electric field, but the central point disappears in an annular plasma and is replaced by an inner wall boundary. In this case, the density peak position becomes a variable in the annulus and the radial transport changes from one direction (outward) in a cylindrical plasma to two directions (outward and inward) in an annular plasma. Hence, the major transport properties of annular plasmas are characterized in the radial dimension and the radial dimension could be reasonably assumed to be frozen as discussed above. The radial transport of collisionless annular plasmas has been previously investigated by using a free-fall model[1] and a fluid model.[16] Our work focuses on the radial transport of annular collisional plasmas with the interest of single-component, electron-positive-ion, and low temperature discharge. The transport of charged particles is described in terms of "diffusion" and "mobility" due to the advantages of unifying the unmagnetized and magnetized plasmas into a simple algebraic form.[11,17] The diffusion represents the momentum balance between the active density gradient and passive collisions, and the mobility represents the balance between the electric field and collisions.[18] By using this representation method, the modelling results for unmagnetized annular plasmas, which is the case of the present study, form the basis of the future study for magnetized plasmas.

The radial transport of an unmagnetized plasma is governed by local ambipolarity for which the ions and electrons have the same drifting flux (non-ambipolarity may arise in the magnetized plasma).[17,19] The light electrons are in quasi-equilibrium in a low temperature plasma (or a weakly ionized plasma) and a one-temperature Maxwellian distribution is assumed for the electrons. The heavy ions are not in equilibrium and their transport behaves following a more complicated process due to the ion-neutral collisions, i.e., elastic ion-neutral collision and resonant charge transfer collision. The effect of long-range Coulomb collisions, i.e., ion-ion and ion-electron collisions, is negligible in a low temperature plasma, and the ion momentum transfer is determined by the ion-neutral collisions of which description depends on the thermalization treatment for ions and neutrals. The combination of cold neutrals and warm ions is

[a]yunchao.zhang@anu.edu.au

normally applied,[10,20] and the opposite case of cold ion beam and warm neutrals has been reported by Fruchtman.[8] Both ions and neutrals remain thermalized in this study and they are connected by using the effective ion temperature.[21,22] The neutral depletion effect[23] is neglected and the neutrals are assumed to be homogeneously distributed. The radial transport of ions is described by three ion mobility based models: a low electric field (LEF) model, an intermediate electric field (IEF) model, and a high electric field (HEF) model. Since the ion diffusion coefficient becomes a complicated electric-field-dependent parameter[18,22] when the ion drift velocity is large compared to the ion thermal velocity (which is the case for IEF and HEF models), its effect was normally neglected in previous HEF studies.[10,11] The present study follows a consistent path and neglects the diffusion effect for ion transport, i.e., the ions behaving an ion-mobility-governed manner.

In the LEF model, the ion-neutral collisions are dominated by the neutral thermal effect and the electric field effect is negligible. The ion mobility coefficient is independent of the electric field and given by the first Chapman-Enskog approximation.[24] The dependency of the ion mobility coefficient on the electric field appears as the electric field strength is increased. At the upper limit of the electric field strength described by the HEF model, the ion-neutral collisions are dominated by the strong electric field and the neutral thermal effect is negligible (cold gas limit). The ion mobility coefficient is inversely proportional to the square root of the electric field strength.[10,25] Both the neutral thermal effect and electric field effect are considered in the IEF model, and the ion-mobility coefficient is expressed in terms of the effective ion temperature.[21,22] To the best of our knowledge, the present paper is the first to use the IEF model to study the ion transport in low temperature plasmas. The total momentum-transfer cross section for ion-neutral collisions (including the elastic ion-neutral collision and resonant charge transfer collision) is approximated to be a constant for the low temperature plasma of interest.[8,11] In a bounded plasma, the LEF dominates the central region of maximum density and the HEF dominates the near-wall presheath region, which accelerates the ions to the Bohm velocity.[26,27] There are two asymmetric presheath regions near the inner and outer walls across an annular plasma. The presheath width extends as the gas pressure decreases,[28] hence the LEF and HEF regimes dominate the high pressure and low pressure plasmas, respectively. This study shows that the IEF model approaches the LEF and HEF models at their respective electric field strength limits and smoothly connects the center region (dominated by the LEF regime) and the near-wall region (dominated by the HEF regime) within an annular plasma.

II. EQUILIBRIUM OF ELECTRONS

The electron flux $\vec{\Gamma}_e = n_e\vec{u}_e$ and ion flux $\vec{\Gamma}_i = n_i\vec{u}_i$, representing the mean drifting motion of electrons and ions, are given as the sum of "diffusion" due to the density gradient $\vec{\nabla}n_{i,e}$ (subscripts "i" and "e" denoting ions and electrons, respectively) and "mobility" due to the electric field $\vec{E}$ (Ref. 17)

$$\vec{\Gamma}_e = -\vec{\vec{D}}_e\vec{\nabla}n_e - n_e\vec{\vec{K}}_e\vec{E}, \tag{1a}$$

$$\vec{\Gamma}_i = -\vec{\vec{D}}_i\vec{\nabla}n_i + n_i\vec{\vec{K}}_i\vec{E}, \tag{1b}$$

where $\vec{\vec{D}}_{i,e}$ and $\vec{\vec{K}}_{i,e}$ are the diffusion tensor and mobility tensor, respectively. The non-diagonal terms are zero in the two tensors due to the absence of magnetic field. The swarm motion of electrons and ions is governed by local ambipolarity of $\vec{\Gamma}_i = \vec{\Gamma}_e$ and the quasi-neutrality $n_i = n_e = n$ is held for the bulk plasma. Combining Eqs. (1b) and (1a) yields

$$(\vec{\vec{D}}_e - \vec{\vec{D}}_i)\vec{\nabla}n + n(\vec{\vec{K}}_e + \vec{\vec{K}}_i)\vec{E} = 0. \tag{2}$$

An electron loses an energy fraction of $\sim m_e/m_g \ll 1$ during an electron-neutral collision, while an ion loses about half of its collisional energy during an ion-neutral collision. As a result, the electron temperature is much higher than the ion temperature $T_e \gg T_i$. The electrons diffuse quickly along the high pressure $(n_e \times eT_e)$ gradient and respond easily to the electric field due to the light inertial mass. In a low temperature plasma, the diffusion and mobility are much faster for electrons than for ions, and the diagonal elements of the diffusion and mobility tensors satisfy $D_e^{(j,j)} \gg D_i^{(j,j)}$ and $K_e^{(j,j)} \gg K_i^{(j,j)}$ $(j = 1, 2, 3$ is the index for tensor elements).[11,17] Equation (2) can be further simplified to give

$$\vec{\vec{D}}_e\vec{\nabla}n + n\vec{\vec{K}}_e\vec{E} = 0, \tag{3}$$

which is equivalent to neglecting $\vec{\Gamma}_e$ in the left hand side (LHS) of Eq. (1a). The above equation shows that the mean drifting motion of electrons is small compared to the motion caused by either the mobility or diffusion. The electrons are in quasi-equilibrium under the forces of electric field and pressure gradient. In this case, the electrons can be described by the Boltzmann relation with the assumption of one-temperature Maxwellian distribution[11,18]

$$n = n_0 \exp\left(\frac{\phi}{T_e}\right), \tag{4}$$

where n_0 and ϕ are the maximum electron (ion) density and the plasma potential, respectively. Applying the gradient operator to both sides of the Boltzmann relation yields

$$\vec{E} = -\vec{\nabla}\phi = -T_e\frac{\vec{\nabla}n}{n}. \tag{5}$$

Substituting this formula into Eq. (3) and considering that the density gradient $\vec{\nabla}n$ should be nontrivial yields

$$\vec{\vec{D}}_e = T_e\vec{\vec{K}}_e, \tag{6}$$

which is the famous "Einstein relation" connecting the mobility and diffusion coefficients in an equilibrium state.

III. RADIAL TRANSPORT OF IONS

The ion flux $\vec{\Gamma}_i$ cannot be neglected for the heavy and non-equilibrium ions in Eq. (1b), and the mean ion drifting

velocity $\vec{u}_i = \frac{\vec{\Gamma}_i}{n}$ is used to define the plasma boundary where it reaches the Bohm velocity. The ions are bounded by an inner wall at radius r_a and an outer wall at radius r_b in an annular plasma. The wall sheath width is normally much smaller than the scale of a plasma and the plasma boundaries are approximately located at the inner and outer walls. The annular plasma can be treated as axially symmetric and no azimuthal flow in the absence of a magnetic field. Hence, on first approximation, a constant axial plasma flux is assumed (frozen axial dimension) and the radial dimension separately solved at the cost of some loss in accuracy (which depends on the specific flow in the assumed frozen dimension) as mentioned in Section I. The radial transport (denoted by the subscript "r") is of primary interest and given by

$$\Gamma_{ir} = -D_{ir}\frac{\mathrm{d}n}{\mathrm{d}r} + nK_{ir}E_r. \tag{7}$$

Combining the Boltzmann relation (5) and the above formula yields

$$\Gamma_{ir} = -(D_{ir} + T_eK_{ir})\frac{\mathrm{d}n}{\mathrm{d}r} = -D_{fr}\frac{\mathrm{d}n}{\mathrm{d}r}, \tag{8a}$$

$$u_{ir} = \frac{\Gamma_{ir}}{n} = -D_{fr}\frac{\mathrm{d}n}{n\mathrm{d}r} = \frac{D_{fr}}{T_e}E_r, \tag{8b}$$

where $D_{fr} = D_{ir} + T_eK_{ir}$ is defined as the effective radial diffusion coefficient. In the LEF regime, the ion diffusion and mobility coefficients D_{ir} and K_{ir} are connected by the linear Einstein relation $D_{ir} = T_iK_{ir}$, and D_{fr} is rewritten as $D_{fr} = (T_i + T_e)K_{ir} \approx T_eK_{ir}$. However, in the IEF and HEF regimes, D_{ir} and K_{ir} violate the linear Einstein relation and a nonlinear generalized Einstein relation (GER) should be used.[21] The diffusion effect was neglected for the HEF model in previous studies[10] for simplicity. The present study follows the same assumption of no diffusion effect for the IEF and HEF models, resulting in the relation

$$D_{fr} = T_eK_{ir}, \tag{9}$$

which is satisfied for all the three models now, and the expression for the radial ion flux Γ_{ir} (8a) is determined by K_{ir}.

A. Ion mobility coefficient

The ion mobility coefficient K_{ir} exhibits different properties in regard to the dominance between the neutral thermal effect and the electric field effect. The formula deduction of K_i is very complicated[18] and not the purpose of this paper. Here, we give a summary of the important results.

In the LEF model for which the electric field effect is small compared to the neutral thermal effect, K_{ir} can be solved by the first Chapman-Enskog approximation[24]

$$K_{ir} = \frac{3(\pi)^{\frac{1}{2}}}{8}\frac{e}{n_g\sigma_m^*}\left(\frac{1}{m_ieT_g}\right)^{\frac{1}{2}}, \tag{10}$$

where T_g is the neutral gas temperature and σ_m^* is a cross section averaged over a distribution of ion-neutral collisional energy ϵ_c

$$\sigma_m^* = \frac{1}{2(eT)^3}\int_0^\infty \sigma_m(\epsilon_c)e^{-\frac{\epsilon_c}{eT}}\epsilon_c^2\,\mathrm{d}\epsilon_c. \tag{11}$$

As σ_m is weakly dependent on the collisional energy of interest in the low temperature plasma, it is approximated to be a constant (hard sphere collision).[8,11] In this case, the distinction between σ_m^* and σ_m disappears, $\sigma_m^* = \sigma_m$.

In the HEF model for which the neutral thermal effect is small compared to the electric field effect (equivalent to the cold gas limit), K_{ir} is inversely proportional to the square root of the electric field strength[25,29]

$$K_{ir} = \xi_H\left(\frac{e}{m_in_g\sigma_m|E_r|}\right)^{\frac{1}{2}}, \tag{12}$$

where the constant ξ_H slightly varies depending on the chosen mobility model and we use $\xi_H = \left(\frac{4}{\pi}\right)^{\frac{1}{2}}$ from the Smirnov model.[25,29] It should be noted that the absolute value of E_r is used in the above formula as E_r can be either positive or negative within an annulus (always positive in a cylinder).

In the IEF model for which neither the neutral thermal effect or the electric field effect is neglected, an effective ion temperature T_{if} is defined to include both effects[21,22]

$$\frac{3}{2}eT_{if} = \frac{3}{2}eT_g + \frac{1}{2}m_gu_{dr}^2. \tag{13}$$

The first term and second term in the right hand side (RHS) represent the contribution of the neutral thermal effect and electric field effect during an ion-neutral collision, respectively. $u_{dr} = K_{ir}E_r$ is a drift velocity purely caused by the electric field (called the electric drift velocity), equivalent to the ion mean drift velocity u_{ir} in a homogeneous plasma. In a non-homogeneous plasma u_{dr} should be less than u_{ir} which includes the influence of both electric field and density gradient. As the diffusion effect (due to the density gradient) is neglected in the present study, $u_{dr} = u_{ir}$ is satisfied by substituting $D_{fr} = T_eK_{ir}$ into Eq. (8b). K_{ir} is given in terms of T_{if} for the IEF model[18]

$$K_{ir} = \xi_I\frac{e}{n_g\sigma_m}\left(\frac{1}{m_ieT_{if}}\right)^{\frac{1}{2}}, \tag{14}$$

which is an implicit equation for K_{ir} and the constant $\xi_I = \frac{3(\pi)^{\frac{1}{2}}}{8}$ is taken from the Mason model.[18,22] In order to make it explicit, two dimensionless parameters are introduced: a dimensionless electric drift velocity $\hat{u}_{dr} = \left(\frac{8}{\pi}\right)^{\frac{1}{2}}\frac{u_{dr}}{u_{th}}$ and a dimensionless electric field parameter $\hat{\varepsilon}_r = \frac{\alpha_I r_b}{T_e}E_r$, where $\alpha_I = \frac{3(2\pi)^{\frac{1}{2}}}{16}\frac{eT_e}{\sigma_mP_{as}}$. Formula (14) is rewritten as

$$\hat{u}_{dr}\left(1 + \frac{2}{3}\hat{u}_{dr}^2\right)^{\frac{1}{2}} = \hat{\varepsilon}_r, \tag{15}$$

which is a quadratic equation of $\hat{u}_{dr}$ and its real solution is given by

$$|\hat{u}_{dr}| = \frac{(3)^{\frac{1}{2}}}{2}\left[\left(1 + \frac{8}{3}\hat{\varepsilon}_r^2\right)^{\frac{1}{2}} - 1\right]^{\frac{1}{2}}. \tag{16}$$

A dimensionless ion mobility coefficient is defined as $\hat{K}_{ir} = \frac{\hat{u}_{dr}}{\hat{\varepsilon}_r}$ and it is proportional to K_{ir} of which the final expression is given by

$$K_{ir} = \frac{(6\pi)^{\frac{1}{2}}}{8}\frac{\bar{u}_{th} r_b}{T_e}\frac{\left[\left(1+\frac{8}{3}\alpha_I^2\hat{E}_r^2\right)^{\frac{1}{2}}-1\right]^{\frac{1}{2}}}{|\hat{E}_r|}. \tag{17}$$

B. Governing equation for radial transport

The radial continuity equation for particle balance is given by

$$\frac{d\Gamma_{ir}}{dr} + \frac{\Gamma_{ir}}{r} - \nu_{iz} n = 0, \tag{18}$$

where $\nu_{iz} = n_g \mu_{iz}$ is the ionization rate, and the rate constant μ_{iz} for one-temperature Maxwellian electrons is given by

$$\mu_{iz} = \left(\frac{8e}{\pi m T_e{}^3}\right)^{1/2}\int_0^\infty \sigma_{iz}(\epsilon_e) e^{-\frac{\epsilon_e}{T_e}}\epsilon_e \, d\epsilon_e, \tag{19}$$

where ϵ_e and σ_{iz} are the electron energy and ionization cross section, respectively.

Substituting the ion flux (8a) into Eq. (18) yields

$$\frac{d^2\hat{n}}{d\hat{r}^2} + \frac{1}{\hat{r}}\frac{d\hat{n}}{d\hat{r}} + \frac{\nu_{iz} r_b^2}{D_{fr}}\hat{n} + \frac{1}{D_{fr}}\frac{dD_{fr}}{d\hat{r}}\frac{d\hat{n}}{d\hat{r}} = 0, \tag{20}$$

where $\hat{n} = \frac{n}{n_0}$ and $\hat{r} = \frac{r}{r_b}$ are the normalized ion density and radial position, respectively. The above equation is normally used in the LEF model for which $\frac{dD_{fr}}{dr} = \frac{dD_{fr}}{dE_r}\frac{dE_r}{dr} = 0$ due to $\frac{dD_{fr}}{dE} = 0$ as shown in formula (10). In the IEF and HEF models, D_{fr} is a function of the electric field with $\frac{dD_{fr}}{dE} \neq 0$, and it is more convenient to express Eq. (20) in terms of the dimensionless electric field $\hat{E}_r = \frac{d\eta}{d\hat{r}}$ as below, where $\eta = -\frac{\phi}{T_e}$ is the dimensionless plasma potential and $\hat{E}_r$ also satisfies $\hat{E}_r = \frac{r_b}{T_e}E_r = -\frac{d\hat{n}}{\hat{n}d\hat{r}}$.

$$\left(1 + \frac{\hat{E}_r}{D_{fr}}\frac{dD_{fr}}{d\hat{E}_r}\right)\frac{d\hat{E}_r}{d\hat{r}} + \frac{\hat{E}_r}{\hat{r}} - \hat{E}_r^2 - \frac{\nu_{iz} r_b^2}{D_{fr}} = 0. \tag{21}$$

Now the radial transport of ions in the annulus can be fully described by adding the boundary conditions, which are given by making the ion mean drift velocity u_{ir} equal to the Bohm velocity $u_B = \left(\frac{eT_e}{m_i}\right)^{1/2}$ at the inner wall r_a and outer wall r_b

$$(u_{ir})_{r=r_a} = -u_B, \ (u_{ir})_{r=r_b} = u_B. \tag{22}$$

Replacing u_{ir} by the equation variables $\hat{n}$ (for Eq. (20)) and $\hat{E}_r$ (for Eq. (21)) using formula (8b) and dimensionless relations defined above yields

$$-\left(\frac{d\hat{n}}{\hat{n}d\hat{r}}\right)_{\hat{r}=\frac{r_a}{r_b}} = (\hat{E}_r)_{\hat{r}=\frac{r_a}{r_b}} = -\frac{u_B r_b}{D_{fr}},$$
$$-\left(\frac{d\hat{n}}{\hat{n}d\hat{r}}\right)_{\hat{r}=1} = (\hat{E}_r)_{\hat{r}=1} = \frac{u_B r_b}{D_{fr}}. \tag{23}$$

IV. ELECTRIC FIELD BASED MODELS

A. LEF model

$D_{fr} = K_{ir} T_e$ is independent of the radial position $\frac{dD_{fr}}{dr} = 0$ for the LEF model as stated above, hence Eq. (20) is reduced to

$$\frac{d^2\hat{n}}{d\hat{r}^2} + \frac{1}{\hat{r}}\frac{d\hat{n}}{d\hat{r}} + \beta_L^2\hat{n} = 0, \tag{24}$$

where β_L satisfies $\beta_L^2 = \frac{\nu_{iz} r_b^2}{D_{fr}} = \frac{2\mu_{iz}\sigma_m \bar{u}_{th}}{3u_B^2}\left(\frac{P_{as}}{eT_g}\right)^2$. $P_{as} = p_g r_b$ ($p_g = eT_g n_g$ is the neutral gas pressure) and $\bar{u}_{th} = \left(\frac{8eT_g}{\pi m_R}\right)^{\frac{1}{2}}$ are the Paschen number for neutral gas and the mean thermal velocity for ion-neutral collisions, respectively. The boundary condition for the LEF model is given by substituting formulas (9) and (10) into (23)

$$-\left(\frac{d\hat{n}}{\hat{n}d\hat{r}}\right)_{\hat{r}=\frac{r_a}{r_b}} = -\frac{u_B r_b}{D_{fr}} = -\frac{2\sigma_m \bar{u}_{th}}{3u_B}\frac{P_{as}}{eT_g} = -\psi_L, \tag{25a}$$

$$-\left(\frac{d\hat{n}}{\hat{n}d\hat{r}}\right)_{\hat{r}=1} = \frac{u_B r_b}{D_{fr}} = \frac{2\sigma_m \bar{u}_{th}}{3u_B}\frac{P_{as}}{eT_g} = \psi_L. \tag{25b}$$

Equation (24) is a Bessel-type equation and its general solution is given by

$$\hat{n} = C_1 J_0(\beta_L \hat{r}) + C_2 Y_0(\beta_L \hat{r}), \tag{26}$$

where J_0 and Y_0 are zero order Bessel functions of the first kind and second kind, and C_1 and C_2 are coefficients to be determined. Substituting the above solution into the boundary condition (25) yields

$$\begin{bmatrix} a_{1,1} & a_{1,2} \\ a_{2,1} & a_{2,2} \end{bmatrix}\begin{bmatrix} C_1 \\ C_2 \end{bmatrix} = 0. \tag{27}$$

The entries in the coefficient matrix are given by

$$a_{1,1} = \beta_L J_1\left(\beta_L \frac{r_a}{r_b}\right) + \psi_L J_0\left(\beta_L \frac{r_a}{r_b}\right),$$
$$a_{1,2} = \beta_L Y_1\left(\beta_L \frac{r_a}{r_b}\right) + \psi_L Y_0\left(\beta_L \frac{r_a}{r_b}\right),$$
$$a_{2,1} = \beta_L J_1(\beta_L) - \psi_L J_0(\beta_L),$$
$$a_{2,2} = \beta_L Y_1(\beta_L) - \psi_L Y_0(\beta_L),$$

where J_1 and Y_1 are first order Bessel functions of the first kind and second kind, respectively. The determinant of the coefficient matrix in Eq. (27) must vanish for a nontrivial solution $\det[\mathbf{a}] = 0$, which determines the electron temperature T_e. The ratio of C_2 to C_1 is given by $\frac{C_2}{C_1} = -\frac{a_{1,1}}{a_{1,2}} = \kappa$, and solution (26) is rewritten as

$$\hat{n} = C_1[J_0(\beta_L \hat{r}) + \kappa Y_0(\beta_L \hat{r})], \tag{28}$$

where C_1 is determined at the peak position of the normalized radial density profile $\hat{r}_p$, satisfying $\frac{d\hat{n}}{d\hat{r}} = 0$ and $\hat{n} = 1$. One argument about the annular solution (28) is its convergence for an infinitesimal inner radius $r_a \to 0$, as the Bessel

function of the second kind diverges near zero. Appendix A proves that the solution is convergent for an infinitesimal r_a due to the adjustable constant κ.

B. HEF model

D_{fr} for the HEF model is obtained using formulas (9) and (12) and its derivative with respect to the variable $\hat{E}_r$ is given by

$$\frac{\mathrm{d}D_{fr}}{\mathrm{d}\hat{E}_r} = -\frac{1}{2}\frac{D_{fr}}{\hat{E}_r}. \tag{29}$$

Substituting formulas (9), (12), and (29) into Eq. (21) yields

$$\frac{\mathrm{d}\hat{E}_r}{\mathrm{d}\hat{r}} + 2\frac{\hat{E}_r}{\hat{r}} - 2\hat{E}_r^2 - 2\beta_H|\hat{E}_r|^{\frac{1}{2}} = 0, \tag{30}$$

where $\beta_H = \frac{\mu_{iz}(\pi\sigma_m)^{\frac{1}{2}}}{2u_B}\left(\frac{P_{as}}{eT_g}\right)^{\frac{3}{2}}$. The boundary condition for the HEF model is given by substituting formulas (9) and (12) into (23)

$$\left(\hat{E}_r\right)_{\hat{r}=\frac{r_a}{r_b}} = -\frac{u_B r_b}{D_{fr}} = -\left(\frac{\pi\sigma_m}{4}\frac{P_{as}}{eT_g}\right)^{\frac{1}{2}}|\hat{E}_r|^{\frac{1}{2}} \;\Rightarrow\; \left(\hat{E}_r\right)_{\hat{r}=\frac{r_a}{r_b}} = -\frac{\pi\sigma_m}{4}\frac{P_{as}}{eT_g}, \tag{31a}$$

$$\left(\hat{E}_r\right)_{\hat{r}=1} = \frac{u_B r_b}{D_{fr}} = \left(\frac{\pi\sigma_m}{4}\frac{P_{as}}{eT_g}\right)^{\frac{1}{2}}|\hat{E}_r|^{\frac{1}{2}} \;\Rightarrow\; \left(\hat{E}_r\right)_{\hat{r}=1} = \frac{\pi\sigma_m}{4}\frac{P_{as}}{eT_g}. \tag{31b}$$

Equation (30) is an Abel-type equation with no analytical solution and the boundary value problem (BVP) for the HEF model is numerically solved using the MATLAB solver,[30] "BVP4C," for which the Hermite-Simpson method was used to solve the ordinary differential equation; an initial solution guess was also evaluated as usually done for most boundary value problems. The validity of this solver has been verified as follow: it was used to numerically solve the LEF model which has an analytical solution as demonstrated in Sec. IV A, and the numerical results calculated from the solver were equal to the results from the analytical solution.

C. IEF model

D_{fr} for the IEF model is obtained using formulas (9) and (17) and its derivative with respect to the variable $\hat{E}_r$ is given by

$$\frac{\mathrm{d}D_{fr}}{\mathrm{d}\hat{E}_r} = -\frac{1}{2}\frac{D_{fr}}{\hat{E}_r}\left[1 - \frac{1}{\left(1+\frac{8}{3}\alpha_I^2\hat{E}_r^2\right)^{\frac{1}{2}}}\right]. \tag{32}$$

Substituting formulas (9), (17), and (32) into to Eq. (21) yields

$$\left[1 + \frac{1}{\left(1+\frac{8}{3}\alpha_I^2\hat{E}_r^2\right)^{\frac{1}{2}}}\right]\frac{\mathrm{d}\hat{E}_r}{\mathrm{d}\hat{r}} + 2\frac{\hat{E}_r}{\hat{r}} - 2\hat{E}_r^2 - 2\beta_I\frac{|\hat{E}_r|}{\left[\left(1+\frac{8}{3}\alpha_I^2\hat{E}_r^2\right)^{\frac{1}{2}} - 1\right]^{\frac{1}{2}}} = 0, \tag{33}$$

where $\beta_I = \left(\frac{32}{3\pi}\right)^{\frac{1}{2}}\frac{\mu_{iz}}{u_{th}}\frac{P_{as}}{eT_g}$. The boundary condition for the IEF model is given by substituting formulas (9) and (17) into (23)

$$\left(\hat{E}_r\right)_{\hat{r}=\frac{r_a}{r_b}} = -\frac{u_B r_b}{D_{fr}} = -\left(\frac{2T_e}{3T_g}\right)^{\frac{1}{2}}\frac{|\hat{E}_r|}{\left[\left(1+\frac{8}{3}\alpha_I^2\hat{E}_r^2\right)^{\frac{1}{2}} - 1\right]^{\frac{1}{2}}}$$

$$\Rightarrow \left(\hat{E}_r\right)_{\hat{r}=\frac{r_a}{r_b}} = -\left(\frac{16}{3\pi}\right)^{\frac{1}{2}}\frac{\sigma_m P_{as}}{eT_e}\left[\left(1+\frac{2T_e}{3T_g}\right)^2 - 1\right]^{\frac{1}{2}}, \tag{34a}$$

$$\left(\hat{E}_r\right)_{\hat{r}=1} = \frac{u_B r_b}{D_{fr}} = \left(\frac{2T_e}{3T_g}\right)^{\frac{1}{2}}\frac{|\hat{E}_r|}{\left[\left(1+\frac{8}{3}\alpha_I^2\hat{E}_r^2\right)^{\frac{1}{2}} - 1\right]^{\frac{1}{2}}}$$

$$\Rightarrow \left(\hat{E}_r\right)_{\hat{r}=1} = \left(\frac{16}{3\pi}\right)^{\frac{1}{2}}\frac{\sigma_m P_{as}}{eT_e}\left[\left(1+\frac{2T_e}{3T_g}\right)^2 - 1\right]^{\frac{1}{2}}. \tag{34b}$$

Equation (33) is a nonlinear ordinary differential equation (ODE) with no analytical solution and the BVP for the IEF model is numerically solved using the same method as that used in the HEF model.

V. MODELLING RESULTS

A. Unification of IEF model

The ion mobility coefficient (17) and the effective ion temperature (13) in the IEF model are unified parameters for the LEF and HEF models. In order to check their universal property, a dimensionless ion mobility coefficient $\hat{K}_{ir}$ and a dimensionless effective ion temperature $\hat{T}_{if}$ are first defined. The former parameter follows the same definition of $\hat{K}_{ir} = \frac{\hat{u}_{dr}}{\hat{\varepsilon}_r}$ in the IEF model for all the three models and the latter parameter is given as follow. Substituting $u_{dr} = \left(\frac{\pi}{8}\right)^{\frac{1}{2}}\bar{u}_{th}\hat{u}_{dr}$ into formula (13) gives $\hat{T}_{if} = \frac{T_{if}}{T_g} = 1 + \frac{2}{3}\hat{u}_{dr}^2$ for the IEF model. Since the first term and second term in the RHS represent the contribution of the neutral thermal effect and electric field effect, respectively, the definition of $\hat{T}_{if}$ can be generalized to the LEF and HEF models: In the LEF model, the electric field effect is negligible and $\hat{T}_{if} = 1$; in the HEF model, the neutral thermal effect is negligible and $\hat{T}_{if} = \frac{2}{3}\hat{u}_{dr}^2$. The expressions for $\hat{K}_{ir}$ and $\hat{T}_{if}$ are summarized as below

$$\text{IEF model}: \quad \hat{K}_{ir} = 1, \quad \hat{T}_{if} = 1, \tag{35a}$$

$$\text{HEF model}: \quad \hat{K}_{ir} = \frac{4}{\pi}\left(\frac{2\pi}{9}\right)^{\frac{1}{4}}|\frac{1}{\hat{\varepsilon}_r}|^{\frac{1}{2}}, \quad \hat{T}_{if} = \frac{2}{3}\left(\hat{K}_{ir}\hat{\varepsilon}_r\right)^2, \tag{35b}$$

$$\text{IEF model}: \quad \hat{K}_{ir} = \frac{(3)^{\frac{1}{2}}}{2}\frac{\left[\left(1+\frac{8}{3}\hat{\varepsilon}_r^2\right)^{\frac{1}{2}}-1\right]^{\frac{1}{2}}}{|\hat{\varepsilon}_r|},$$
$$\hat{T}_{if} = 1+\frac{2}{3}\left(\hat{K}_{ir}\hat{\varepsilon}_r\right)^2. \tag{35c}$$

Figures 1(a) and 1(b) present the $\hat{K}_{ir}(|\hat{\varepsilon}_r|)$ curve and $\hat{T}_{if}(|\hat{\varepsilon}_r|)$ curve for the LEF model (dashed-dotted line), the IEF model (solid line), and the HEF model (dashed line). Figure 1(a) shows that $\hat{K}_{ir}$ is a decreasing function of $|\hat{\varepsilon}_r|$ for the three models, and Figure 1(b) shows that $\hat{T}_{if}$ is an increasing function of $|\hat{\varepsilon}_r|$. In both Figures 1(a) and 1(b), the IEF curve is consistent with the LEF curve for the range of $|\hat{\varepsilon}_r| < 0.1$, and it is consistent with the HEF curve for the range of $|\hat{\varepsilon}_r| > 10$. Hence, $\hat{K}_{ir}$ and $\hat{T}_{if}$ for the IEF model are unified parameters for the other two models at their respective electric field strength limits. The IEF transport equation (33) also has a universal property: it is reduced to the LEF transport equation (24) when $\hat{E}_r$ approaches zero, and it is reduce the HEF transport equation (30) when $\hat{E}_r$ approaches infinity. A detailed proof is given in Appendix B.

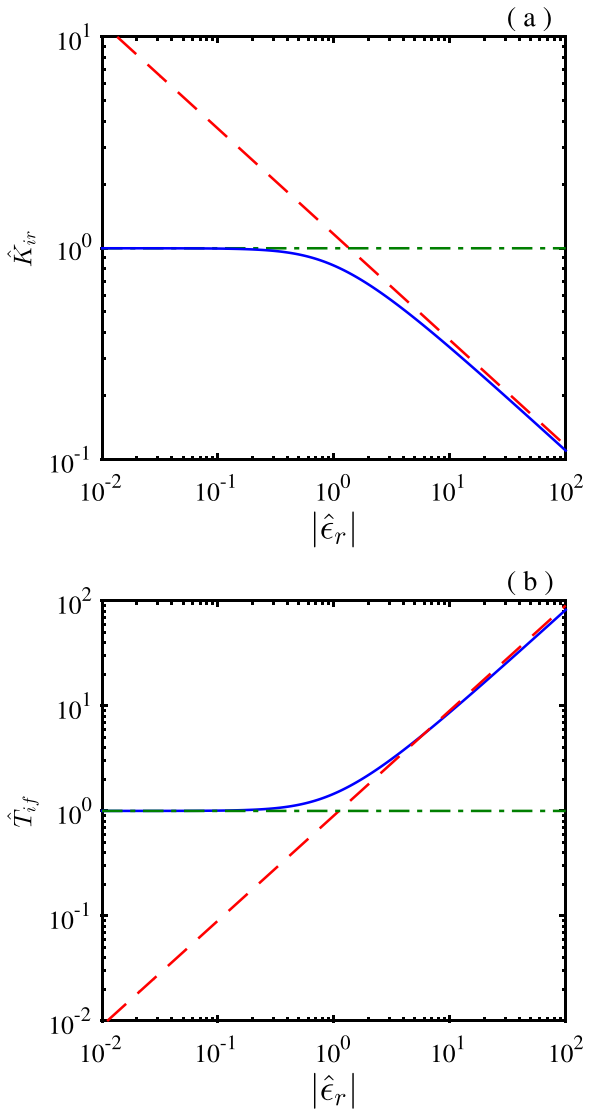

FIG. 1. (a) $\hat{K}_{ir}(|\hat{\varepsilon}_r|)$ curve obtained by the LEF model (dashed-dotted line), the IEF model (solid line), and the HEF model (dashed line). (b) $\hat{T}_{if}(|\hat{\varepsilon}_r|)$ curve obtained by the LEF model (dashed-dotted line), the IEF model (solid line), and the HEF model (dashed line).

B. Numerical results for argon plasma

We illustrate the annular modelling results for a low temperature argon plasma. The input parameters are the Paschen number P_{as} and the annular geometry ratio $\frac{r_a}{r_b}$; the output parameters are the normalized ion density $\hat{n}$, the boundary loss coefficient L_R (defined later in formula (37)), and the electron temperature T_e. The argon has an atomic mass of $m_g = 39.95\,\text{u}$ ($\text{u} = 1.6605 \times 10^{-27}\,\text{kg}$ is the atomic mass unit) and a neutral gas temperature of $T_g = 0.026\,\text{V}$ (room temperature). The ionization cross section σ_{iz} formulated by Phelps[31] is used for the argon ionization calculation (19)

$$\sigma_{iz} = \frac{970}{(\epsilon+70)^2}(\epsilon-15.8) + 0.06e^{-\frac{\epsilon}{9}}(\epsilon-15.8)^2, \tag{36}$$

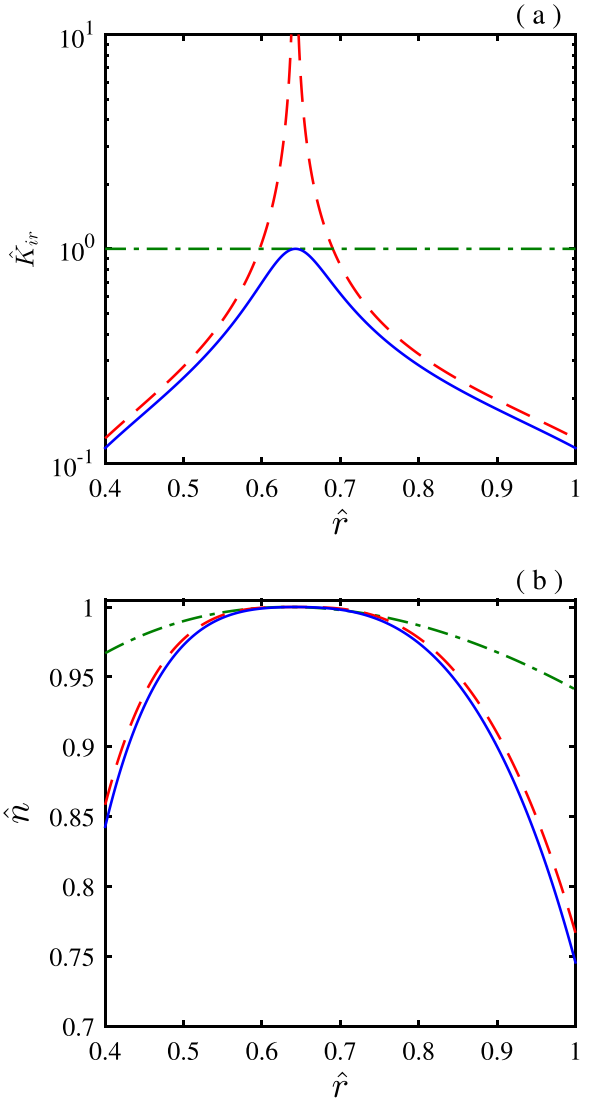

FIG. 2. (a) Radial profile of $\hat{K}_{ir}$ for an annular geometry ratio of $\frac{r_a}{r_b} = 0.4$ with a Paschen number of $P_{as} = 0.01\,\text{Torr cm}$ obtained by the LEF model (dashed-dotted line), the IEF model (solid line), and the HEF model (dashed line). (b) Radial profile of $\hat{n}$ for $\frac{r_a}{r_b} = 0.4$ with $P_{as} = 0.01\,\text{Torr cm}$ obtained by the LEF model (dashed-dotted line), the IEF model (solid line), and the HEF model (dashed line).

where σ_{iz} is in the unit of $10^{-20}\,\mathrm{m}^2$. A total momentum-transfer cross section (including the elastic ion-neutral collision and resonant charge transfer collision) of $\sigma_m = 10^{-18}\,\mathrm{m}^2$ is used for ion-neutral collisions in the low temperature argon plasma.[11] As σ_m is a constant, P_{as} is proportional to the Knudsen number $K_n = \frac{\lambda_i}{r_b}$, where λ_i is the ion mean free path. It should be noted that the collisional annular model has a validity limit of $K_n \lesssim \frac{r_b - r_a}{r_b}$. The annular plasma becomes collisionless when $K_n \gg \frac{r_b - r_a}{r_b}$ and the present modelling will be invalid for the collisionless scenario.

Figures 2(a) and 2(b) present the radial profile of $\hat{K}_{ir}$ and $\hat{n}$ for a typical annular geometry ratio of $\frac{r_a}{r_b} = 0.4$ with a low P_{as} number of $P_{as} = 0.01\,\mathrm{Torr}\cdot\mathrm{cm}$ (for which λ_i is comparable to the annular width $(r_b - r_a)$ with $K_n \sim \frac{1}{3}$, $\frac{r_b - r_a}{r_b} = 0.6$) obtained by the LEF model (dashed-dotted line), the IEF model (solid line), and the HEF model (dashed line). Figure 2(a) shows that the IEF profile reaches its maximum at $\hat{r} \sim 0.64$ and the HEF profile approaches infinity at $\hat{r} \sim 0.64$, indicating a small electric field nearby. The LEF profile remains constant across the radial dimension due to the neglect of electric field effect (similar phenomenon as shown in Figure 1). Figure 2(b) shows that the $\hat{n}$ profiles obtained by the three models are asymmetric around a similar peak position of $\hat{r}_p \sim 0.64$, which is related to the peak position of IEF and HEF profiles in Figure 2(a). The boundary-to-maximum density ratio is about $\hat{n}_{a,b} \sim 0.95$ for the LEF model and ~0.8 for the IEF and HEF models. Figures 3(a) and 3(b) present the radial profile of $\hat{K}_{ir}$ and $\hat{n}$ for $\frac{r_a}{r_b} = 0.4$ with a high P_{as} number of $P_{as} = 1.0\,\mathrm{Torr\,cm}$ (for which λ_i is small compared to $(r_b - r_a)$ with $K_n \sim \frac{1}{300}$) obtained by the LEF model (dashed-dotted line), the IEF model (solid line), and the HEF model (dashed line). Figure 3(a) shows that the IEF profile reaches its maximum at $\hat{r} \sim 0.67$ and the HEF profile approaches infinity at $\hat{r} \sim 0.66$ (not completely shown in Figure 3(a) to maintain visual clarity). Figure 3(b) shows that the $\hat{n}$ profiles are asymmetric around a similar peak position of $\hat{r}_p \sim 0.67$. The boundary density ratio is about $\hat{n}_{a,b} \sim 0.1$ for the three models.

Figures 2(a) and 3(a) show that the $\hat{K}_{ir}$ profile of the IEF model is consistent with that of the LEF model in the central peak region (or LEF regime) and consistent with that of the HEF model in the boundary region (or HEF regime). The IEF $\hat{K}_{ir}$ profile's central consistency with the LEF profile dominates for a high P_{as} number (Figure 3(a)) and its boundary consistency with the HEF profile dominates for a low P_{as} number (Figure 2(a)). The universal property of radial $\hat{K}_{ir}$ profile obtained by the IEF model in Figures 2 and 3 is consistent with the $\hat{K}_{ir}(|\hat{\varepsilon}_r|)$ curve in Figure 1(a). The IEF model gives more accurate results of $\hat{K}_{ir}$, $\hat{T}_{if}$, and $\hat{n}$ (determined by the expression of $\hat{K}_{ir}$) than the LEF and HEF models over the entire electric field strength range and it will be used to further investigate the radial transport properties of the annular plasma.

The shape of radial $\hat{n}$ profile across the annulus is characterized by the density peak position $\hat{r}_p$ and boundary density ratios. An annular boundary loss coefficient L_R, similar to the boundary density parameters h_R and h_l for the cylindrical and plane-parallel plasmas,[11] is defined for an annular plasma as

$$L_R = \frac{r_a}{r_b}\hat{n}_a + \hat{n}_b. \tag{37}$$

It is a generalized boundary density ratio and can be used to estimate the value of the maximum density n_0 by considering power balance.[8,11] Figures 4(a) and 4(b) present the $\hat{r}_p\left(\frac{r_a}{r_b}\right)$ curve and $L_R\left(\frac{r_a}{r_b}\right)$ curve obtained by the IEF model for different P_{as} numbers of $P_{as} = 0.01\,\mathrm{Torr\,cm}$ (dashed-dotted line), $0.1\,\mathrm{Torr\,cm}$ (solid line), and $1.0\,\mathrm{Torr\,cm}$ (dashed line). Figure 4(a) shows that $\hat{r}_p$ is a monotonically increasing function of $\frac{r_a}{r_b}$ and the variation is stronger in the low $\frac{r_a}{r_b}$ range. $\hat{r}_p$ approaches to the middle of the annulus (shown as the dotted line) when $\frac{r_a}{r_b} > 0.8$. $\hat{r}_p$ is greater for a higher P_{as} number compared to a lower P_{as} number. Figure 4(b) shows that L_R is also a monotonically increasing function of $\frac{r_a}{r_b}$ and the

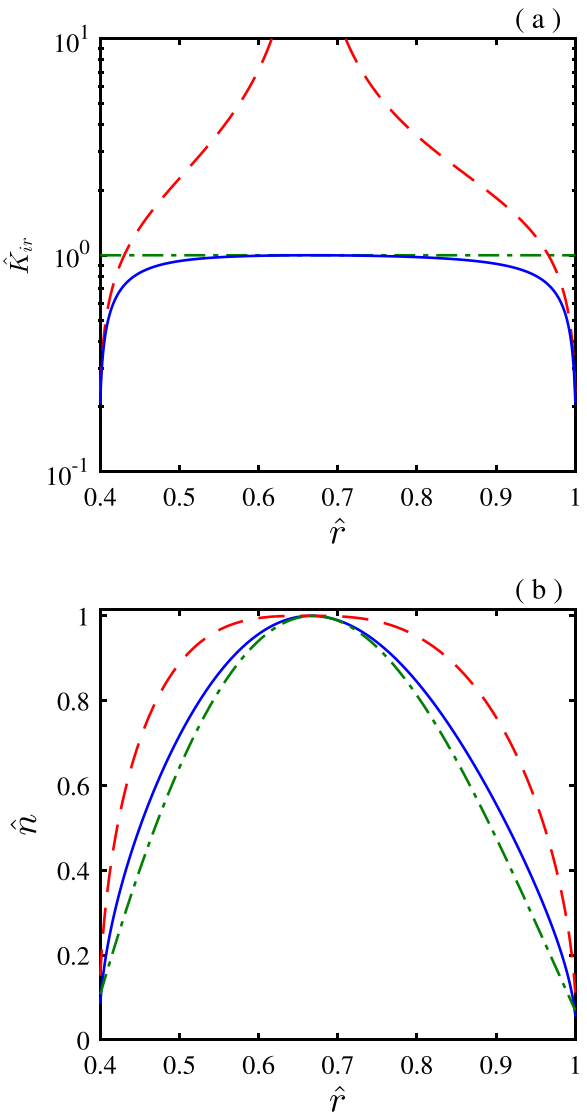

FIG. 3. (a) Radial profile of $\hat{K}_{ir}$ for an annular geometry ratio of $\frac{r_a}{r_b} = 0.4$ with a Paschen number of $P_{as} = 1.0\,\mathrm{Torr\,cm}$ obtained by the LEF model (dashed-dotted line), the IEF model (solid line), and the HEF model (dashed line). (b) Radial profile of $\hat{n}$ for $\frac{r_a}{r_b} = 0.4$ with $P_{as} = 1.0\,\mathrm{Torr\,cm}$ obtained by the LEF model (dashed-dotted line), the IEF model (solid line), and the HEF model (dashed line).

variation is greater in the high $\frac{r_a}{r_b}$ range. In the low $\frac{r_a}{r_b}$ range L_R increases faster for a higher P_{as} number, while in the high $\frac{r_a}{r_b}$ range L_R increases faster for a lower P_{as} number. Contrarily to $\hat{r}_p$ in Figure 4(a), L_R is greater for a lower P_{as} number than for a higher P_{as} number.

Figures 5(a) and 5(b) present the $\hat{r}_p(P_{as})$ curve and $L_R(P_{as})$ curve obtained by the IEF model for different annular geometry ratios of $\frac{r_a}{r_b} = 0.2$ (dashed-dotted line), 0.4 (solid line), 0.6 (dashed line), and 0.8 (dotted line). Figure 5(a) shows that $\hat{r}_p$ is an increasing function of P_{as} (consistent with the results in Figure 4(a)) and the total increment $\Delta\hat{r}_p$ over the variable range of 10^{-3} Torr cm $< P_{as} <$ 10 Torr cm is reduced for higher $\frac{r_a}{r_b}$, with an increment of $\Delta\hat{r}_p \sim 0.08$ for $\frac{r_a}{r_b} = 0.2$ and $\Delta\hat{r}_p \sim 0.003$ for $\frac{r_a}{r_b} = 0.8$. Figure 5(b) shows that L_R is a reversed-"S"-shape decreasing function of P_{as} (consistent with the results in Figure 4(b)) and the variation is stronger in the middle range between ~0.01 Torr cm and ~1 Torr cm than in the edge ranges. L_R approaches to zero when P_{as} reaches a high value of $P_{as} \sim 10$ Torr cm. Figures 5(a) and 5(b) show that $\hat{r}_p$ is a more robust parameter than L_R as a function of the P_{as} number.

Figure 6(a) presents the $T_e\left(\frac{r_a}{r_b}\right)$ curve obtained by the IEF model for different P_{as} numbers of $P_{as} = 0.01$ Torr cm (dashed-dotted line), 0.1 Torr cm (solid line), and 1.0 Torr cm (dashed line). T_e is an increasing function of $\frac{r_a}{r_b}$ and the variation is stronger in the high $\frac{r_a}{r_b}$ range. The $T_e\left(\frac{r_a}{r_b}\right)$ curve exhibits higher values and increases faster for a lower P_{as} number, with an increment of $\Delta T_e \sim 12.0$ eV for $P_{as} = 0.01$ Torr cm, $\Delta T_e \sim 2.3$ eV for $P_{as} = 0.1$ Torr cm, and $\Delta T_e \sim 0.9$ eV for $P_{as} = 1.0$ Torr cm over the range of $0.01 < \frac{r_a}{r_b} < 0.9$. Figure 6(b) presents the $T_e(P_{as})$ curve obtained by the IEF model for different annular geometry ratios of $\frac{r_a}{r_b} =$ 0.2 (dashed-dotted line), 0.4 (solid line), 0.6 (dashed line), and 0.8 (dotted line). T_e is a decreasing

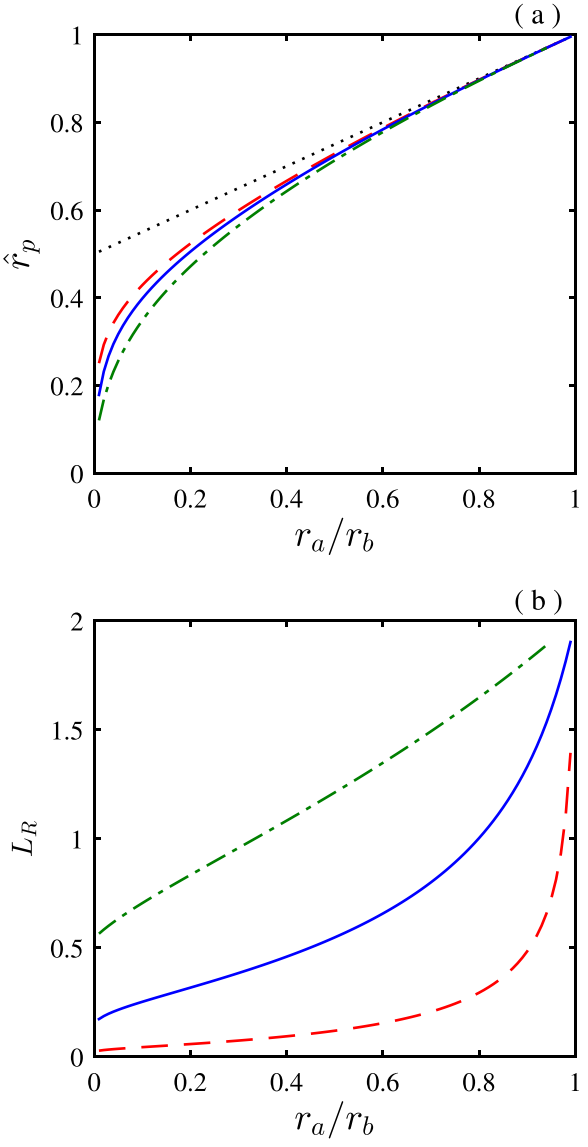

FIG. 4. (a) $\hat{r}_p\left(\frac{r_a}{r_b}\right)$ curve obtained by the IEF model for different Paschen numbers of $P_{as} = 0.01$ (dashed line), 0.1 (solid line), and 1 (dashed-dotted line). The dotted-line shows the normalized middle position of the annulus as a function of $\frac{r_a}{r_b}$. (b) $L_R\left(\frac{r_a}{r_b}\right)$ curve obtained by the IEF model for different Paschen numbers of $P_{as} = 0.01$ (dashed line), 0.1 (solid line), and 1 (dashed-dotted line).

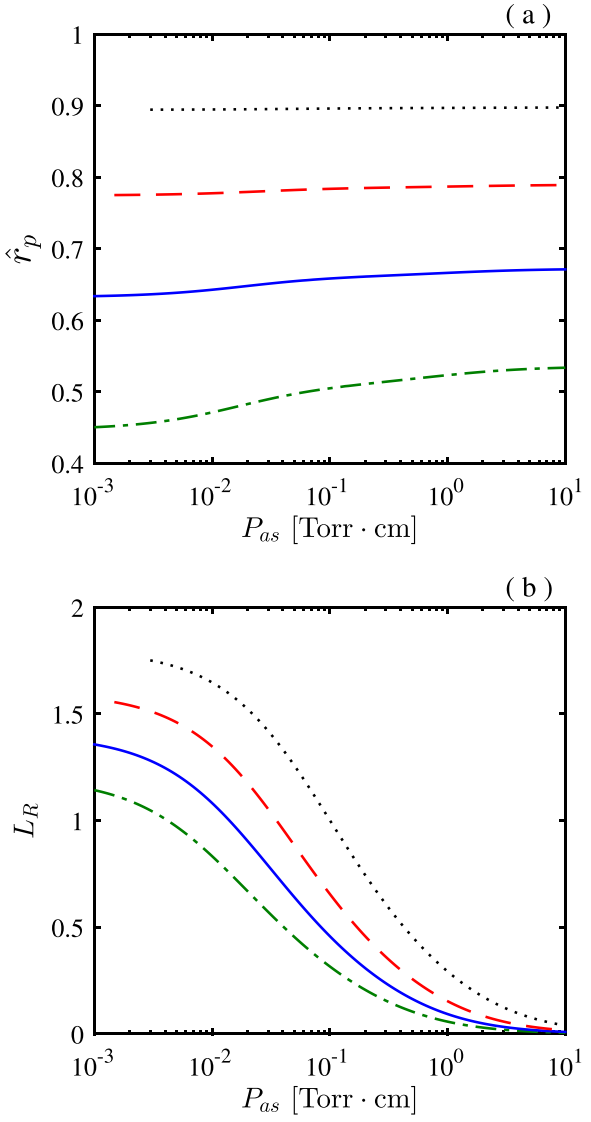

FIG. 5. (a) $\hat{r}_p(P_{as})$ curve obtained by the IEF model for different annular geometry ratios of $\frac{r_a}{r_b} = 0.2$ (dashed line), 0.4 (solid line), 0.6 (dashed-dotted line), and 0.8 (dotted line). (b) $L_R(P_{as})$ curve obtained by the IEF model for different annular geometry ratios of $\frac{r_a}{r_b} = 0.2$ (dashed line), 0.4 (solid line), 0.6 (dashed-dotted line), and 0.8 (dotted line).

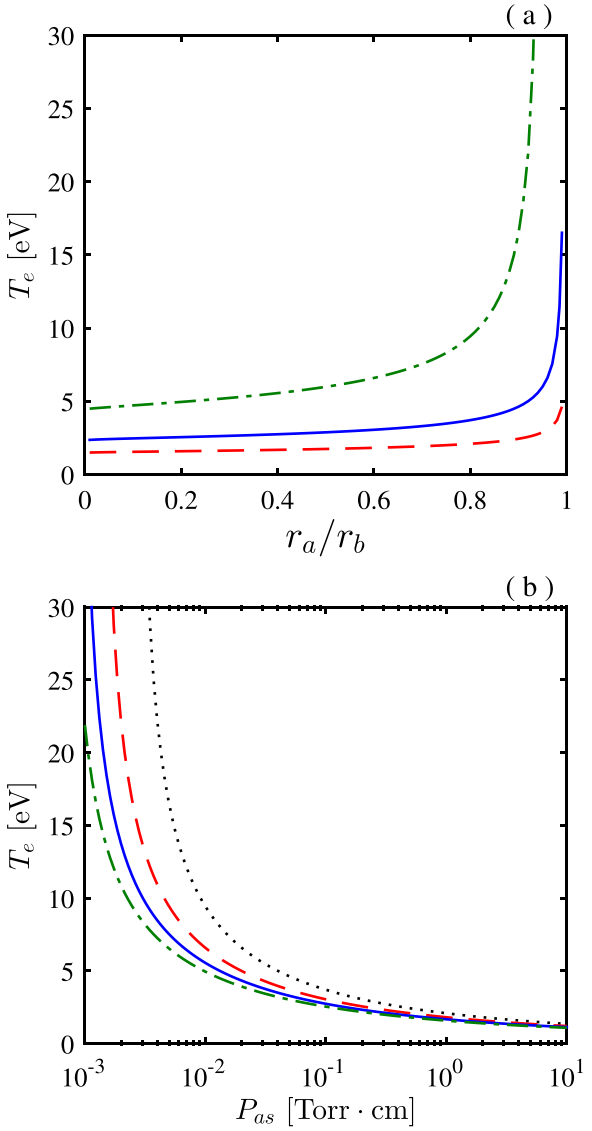

FIG. 6. (a) $T_e\left(\frac{r_a}{r_b}\right)$ curve obtained by the IEF model for different Paschen numbers of $P_{as} = 0.01$ (dashed line), 0.1 (solid line), and 1 (dashed-dotted line). (b) $T_e(P_{as})$ curve obtained by the IEF model for different annular geometry ratios of $\frac{r_a}{r_b} = 0.2$ (dashed line), 0.4 (solid line), 0.6 (dashed-dotted line), and 0.8 (dotted line).

function of P_{as} and the variation is more pronounced over the low P_{as} number range. In the high P_{as} number range of $P_{as} > 1$ Torr cm, T_e approaches a similar value for different annular geometries, with $T_e \sim 1.8$ eV at $P_{as} = 1$ Torr cm and $T_e \sim 1.2$ eV at $P_{as} = 10$ Torr cm. The $T_e(P_{as})$ curve shows higher values and decreases faster for a higher $\frac{r_a}{r_b}$, with a drop of $\Delta T_e \sim -3.4$ eV for $\frac{r_a}{r_b} = 0.2$, $\Delta T_e \sim -3.9$ eV for $\frac{r_a}{r_b} = 0.4$, $\Delta T_e \sim -4.8$ eV for $\frac{r_a}{r_b} = 0.6$, and $\Delta T_e \sim -7.5$ eV for $\frac{r_a}{r_b} = 0.8$ over the range of 0.01 Torr cm $< P_{as} <$ 1.0 Torr cm. Figures 4(b), 5(b), 6(a), and 6(b) show that T_e has a positive correlation with L_R with respect to the variables $\frac{r_a}{r_b}$ and P_{as}.

VI. SUMMARY

The radial transport properties of low temperature annular plasmas were investigated. The electrons were in quasi-equilibrium and governed by the Boltzmann relation. The annular modelling given in this work is ion-mobility-based (the diffusion effect was neglected as mentioned above), and its applicable range is determined by the accuracy of the ion mobility coefficient. The mobility coefficient calculated by the LEF or HEF model has a good accuracy at the low or high electric field limit for which the validity has been verified in previous studies for cylindrical and plane parallel plasmas. The IEF model presents a more unified mobility coefficient over the entire electric field strength range and approaches the results of LEF and HEF models at the respective electric field limits as shown in Section V. Hence, the IEF model gives more accurate results compared to the LEF and HEF models over the entire electric field range. Future studies will aim at comparing the IEF results to other experimental or computational studies, which, to the best of our knowledge, are not yet readily available in the literature.

The annular modelling was applied to a low temperature argon plasma. The normalized radial density profile obtained by the IEF model joins the LEF model in the central peak region and joins the HEF model in the boundary region. The radial profile is asymmetric around the peak position with the latter found closer to the inner wall. The density peak position is an increasing function of the annular geometry ratio and Paschen number. An annular boundary loss coefficient is defined to characterize the boundary density ratios, and it is an increasing function of the annular geometry ratio and a decreasing function of the Paschen number. More ions are lost to the walls for a higher annular geometry ratio, and the radial transport of ions is more effective for a low Paschen number (high Knudsen number) due to less ion-neutral collisions. The electron temperature has a positive correlation with the annular boundary loss coefficient with respect to the variable annular geometry ratio and Paschen number. When the boundary loss of ions is enhanced, the electron temperature increases to provide more ionization and satisfies particle balance.

APPENDIX A: INFINITESIMAL INNER RADIUS LIMIT OF LEF MODEL

The convergence of LEF solution (28) at an infinitesimal inner boundary $\hat{r} = \frac{r_a}{r_b} \to 0$ is determined by the second term $\kappa Y_0(\beta_L \hat{r})$. Define a function $F(\hat{r})$ as

$$F(\hat{r}) = \kappa Y_0(\beta \hat{r}) = -\frac{\beta_L J_1\left(\beta_L \frac{r_a}{r_b}\right) + \psi_L J_0\left(\beta_L \frac{r_a}{r_b}\right)}{\beta_L Y_1\left(\beta_L \frac{r_a}{r_b}\right) + \psi_L Y_0\left(\beta_L \frac{r_a}{r_b}\right)} Y_0[\beta \hat{r}]. \tag{A1}$$

When $\hat{r} = \frac{r_a}{r_b}$ approaches zero, (1) J_0 and J_1 approach unity and zero, respectively, and (2) Y_1 diverges faster than Y_0 with $\frac{Y_1}{Y_0} \to +\infty$. Then, $F\left(\frac{r_a}{r_b}\right)$ can be rewritten as

$$\left[F\left(\frac{r_a}{r_b}\right)\right]_{r_a \to 0} = \frac{1}{\frac{\beta_L}{\psi_L}\frac{Y_1\left(\beta_L \frac{r_a}{r_b}\right)}{Y_0\left(\beta_L \frac{r_a}{r_b}\right)} + 1} \sim 0. \tag{A2}$$

Hence, the annular solution (28) is convergent and reduced to the classic cylindrical solution of $\hat{n} = J_0(\beta_L \hat{r})$ for an infinitesimal inner boundary.

APPENDIX B: ELECTRIC FIELD LIMITS OF IEF MODEL

At the limit of infinitesimal electric field, $\hat{E}_r \to 0$, $\left(1 + \frac{8}{3}\alpha_I^2 \hat{E}_r^2\right)^{\frac{1}{2}}$ can be approximated by its first order Taylor expansion $\left(1 + \frac{4}{3}\alpha_I^2 \hat{E}_r^2\right)$. Substituting this approximation into Eq. (33) and considering $\alpha_I |\hat{E}_r| \ll 1$ yields

$$\frac{d\hat{E}_r}{d\hat{r}} + \frac{\hat{E}_r}{\hat{r}} - \hat{E}_r^2 - \beta_I^* = 0, \tag{B1}$$

where $\beta_I^* = \frac{(3)^{\frac{1}{2}}}{2}\frac{\beta_L}{\alpha_I} = \frac{2\mu_{iz}\sigma_m \bar{u}_{th}}{3u_B^2}\left(\frac{P_{as}}{eT_g}\right)^2$ is equal to β_L^2. Substituting $\hat{E}_r = -\frac{d\hat{n}}{\hat{n}d\hat{r}}$ into the above equation gives

$$\frac{d^2\hat{n}}{d\hat{r}^2} + \frac{1}{\hat{r}}\frac{d\hat{n}}{d\hat{r}} + \beta_I^* \hat{n} = 0, \tag{B2}$$

which is exactly the LEF transport equation (24) at the low electric field strength limit.

At the other limit of infinite electric field, $\hat{E}_r \to \infty$, $\left(1 + \frac{8}{3}\alpha_I^2 \hat{E}_r^2\right)^{\frac{1}{2}}$ is approximated by $\left(\frac{8}{3}\right)^{\frac{1}{2}}\alpha_I |\hat{E}_r|$. Substituting this approximation into Eq. (33) and considering $\alpha_I |\hat{E}_r| \gg 1$ yields

$$\frac{d\hat{E}_r}{d\hat{r}} + 2\frac{\hat{E}_r}{\hat{r}} - 2\hat{E}_r^2 - 2\beta_I^{**}|\hat{E}_r|^{\frac{1}{2}} = 0, \tag{B3}$$

where $\beta_I^{**} = \left(\frac{3}{8}\right)^{\frac{1}{4}}\frac{\beta_I}{(\alpha_I)^{\frac{1}{2}}} = \frac{4}{3}\left(\frac{12}{\pi^3}\right)^{\frac{1}{4}}\frac{\mu_{iz}(\pi\sigma_m)^{\frac{1}{2}}}{2u_B}\left(\frac{P_{as}}{eT_g}\right)^{\frac{3}{2}}$ is 5% higher than β_H, hence the IEF transport equation (B3) is a good approximation to the HEF transport equation (30) at the high electric field strength limit.

[1]L. Tonks and I. Langmuir, "A general theory of the plasma of an arc," Phys. Rev. **34**, 876 (1929).
[2]J. F. Waymouth, "Perturbation of a plasma by a probe," Phys. Fluids **7**, 1843 (1964).
[3]G. Cunge, B. Crowley, D. Vender, and M. M. Turner, "Anomalous skin effect and collisionless power dissipation in inductively coupled discharges," J. Appl. Phys. **89**, 3580 (2001).
[4]V. N. Volynets, W. Park, Y. N. Tolmachev, V. G. Pashkovsky, and J. Yoo, "Spatial variation of plasma parameters and ion acceleration in an inductive plasma system," J. Appl. Phys. **99**, 043302 (2006).
[5]Y. Zhang, C. Charles, and R. Boswell, "Transport of ion beam in an annular magnetically expanding helicon double layer thruster," Phys. Plasmas **21**, 063511 (2014).
[6]M. G. Kong, G. Kroesen, G. Morfill, T. Nosenko, T. Shimizu, J. van Dijk, and J. L. Zimmermann, "Plasma medicine: An introductory review," New J. Phys. **11**, 115012 (2009).
[7]S. Hofmann, A. F. H. van Gessel, T. Verreycken, and P. Bruggeman, "Power dissipation, gas temperatures and electron densities of cold atmospheric pressure helium and argon rf plasma jets," Plasma Sources Sci. Technol. **20**, 065010 (2011).
[8]A. Fruchtman, G. Makrinich, and J. Ashkenazy, "Two-dimensional equilibrium of a low temperature magnetized plasma," Plasma Sources Sci. Technol. **14**, 152 (2005).
[9]N. Sternberg and V. Godyak, "Two-dimensional cylindrical plasma for intermediate gas pressures," Plasma Sources Sci. Technol. **20**, 015018 (2011).
[10]V. A. Godyak, *Soviet Radio Frequency Discharge Research* (Delphic Associates, Falls Church, VA, 1986).
[11]M. A. Lieberman and A. J. Lichtenberg, *Principles of Plasma Discharges and Materials Processing*, 2nd ed. (John Wiley & Sons, New York, 2005).
[12]J. E. Allen, "The plasma boundary in a magnetic field," Contrib. Plasma Phys. **48**, 400 (2008).
[13]S. Ashida, M. R. Shimand, and M. A. Lieberman, "Measurements of pulsed-power modulated argon plasmas in an inductively coupled plasma source," J. Vac. Sci. Technol., A **14**, 391 (1996).
[14]G. H. Kim, H. C. Lee, and C. W. Chung, "Experimental investigation of edge-to-center density ratio in inductively coupled plasmas," Phys. Plasmas **17**, 073504 (2010).
[15]H. C. Lee and C. W. Chung, "Experimental measurements of spatial plasma potentials and electron energy distributions in inductively coupled plasma under weakly collisional and nonlocal electron kinetic regimes," Phys. Plasmas **19**, 033514 (2012).
[16]E. Ahedo, "Radial macroscopic model of a plasma flowing along annular dielectric walls," Phys. Plasmas **9**, 3178 (2002).
[17]A. Fruchtman, "Ambipolar and nonambipolar cross-field diffusions," Plasma Sources Sci. Technol. **18**, 025033 (2009).
[18]E. A. Mason and E. W. McDaniel, *Transport Properties of Ions in Gases* (John Wiley & Sons, New York, 1988).
[19]A. P. Zhilinskii and L. D. Tsendin, "Collisional diffusion of a partially-ionized plasma in a magnetic field," Sov. Phys. Usp. **23**, 331 (1980).
[20]B. N. Breizman and A. V. Arefiev, "Ion kinetics in a magnetized plasma source," Phys. Plasmas **9**, 1015 (2002).
[21]G. H. Wannier, "Motion of gaseous ions in strong electric fields," Bell Syst. Tech. J. **32**, 170 (1953).
[22]L. A. Viehland and E. A. Mason, "Gaseous ion mobility and diffusion in electric fields of arbitrary strength," Ann. Phys. **110**, 287 (1977).
[23]L. Liard, J. L. Raimbault, J. M. Rax, and P. Chabert, "Plasma transport under neutral gas depletion conditions," J. Phys. D: Appl. Phys. **40**, 5192 (2007).
[24]S. Chapman and T. G. Cowling, *The Mathematical Theory of Non-Uniform Gases*, 3rd ed. (Cambridge University Press, London, 1970).
[25]H. S. Hahn and E. A. Mason, "Field dependence of gaseous-ion mobility: Theoretical tests of approximate formulas," Phys. Rev. A **6**, 1573 (1972).
[26]D. Bohm, "Minimum ionic kinetic energy for a stable sheath," in *The Characteristics of Electrical Discharges in Magnetic Fields*, edited by A. Guthrie and R. Wakerling (McGraw-Hill, New York, 1949), Chap. 3.
[27]J. E. Allen, "The plasma–sheath boundary: its history and Langmuir's definition of the sheath edge," Plasma Sources Sci. Technol. **18**, 014004 (2009).
[28]K. U. Riemann, "Plasma and sheath," Plasma Sources Sci. Technol. **18**, 014006 (2009).
[29]B. M. Smirnov, *Physics of Weakly Ionized Gases* (Mir Publishers, Moscow, 1981).
[30]L. F. Shampine, I. Gladwell, and S. Thompson, *Solving ODEs with MATLAB* (Cambridge University Press, New York, NY, 2003).
[31]A. V. Phelps and Z. L. Petrovic, "Cold-cathode discharges and breakdown in argon: surface and gas phase production of secondary electrons," Plasma Sources Sci. Technol. **8**, R21 (1999).